PCCP

ROYAL SOCIETY OF CHEMISTRY

PAPER

View Article Online
View Journal | View Issue

Cite this: *Phys. Chem. Chem. Phys.*, 2022, **24**, 14640

The superior effect of edge functionalization relative to basal plane functionalization of graphene in enhancing the thermal conductivity of polymer–graphene nanocomposites – a combined molecular dynamics and Green's functions study

Rajmohan Muthaiah, *[a] Fatema Tarannum, [a] Swapneel Danayat,[a] Roshan Sameer Annam,[a] Avinash Singh Nayal,[a] N. Yedukondalu [b] and Jivtesh Garg [a]

To achieve polymer–graphene nanocomposites with high thermal conductivity (k), it is critically important to achieve efficient thermal coupling between graphene and the surrounding polymer matrix through effective functionalization schemes. In this work, we demonstrate that edge-functionalization of graphene nanoplatelets (GnPs) can enable a larger enhancement of effective thermal conductivity in polymer–graphene nanocomposites relative to basal plane functionalization. Effective thermal conductivity for the edge case is predicted, through molecular dynamics simulations, to be up to 48% higher relative to basal plane bonding for 35 wt% graphene loading with 10 layer thick nanoplatelets. The beneficial effect of edge bonding is related to the anisotropy of thermal transport in graphene, involving very high in-plane thermal conductivity (~2000 W m^{-1} K^{-1}) compared to the low out-of-plane thermal conductivity (~10 W m^{-1} K^{-1}). Likewise, in multilayer graphene nanoplatelets (GnPs), the thermal conductivity across the layers is even lower due to the weak van der Waals bonding between each pair of layers. Edge functionalization couples the polymer chains to the high in-plane thermal conduction pathway of graphene, thus leading to overall high thermal conductivity of the composite. Basal-plane functionalization, however, lowers the thermal resistance between the polymer and the surface graphene sheets of the nanoplatelet only, causing the heat conduction through inner layers to be less efficient, thus resulting in the basal plane scheme to be outperformed by the edge scheme. The present study enables fundamentally novel pathways for achieving high thermal conductivity polymer nanocomposites.

Received 10th January 2022,
Accepted 1st May 2022

DOI: 10.1039/d2cp00146b

rsc.li/pccp

1. Introduction

High thermal conductivity (k) polymer materials can improve thermal management in a wide range of applications such as automotive control units,[1] batteries,[2–4] solar panels,[5] electronic packaging,[6] electronic cooling,[7] *etc.* A promising approach to enhance the thermal conductivity of polymers is molecular orientation,[8–10] and the addition of high k fillers[11–17] is performed to improve the overall thermal conductivity of polymer nanocomposites. However, the benefits of adding high k fillers are limited due to the large interface thermal resistance between the polymer and fillers in the range of 10^{-8} to 10^{-7} m^2 kW^{-1} [18,19] due to phonon mismatch between these two. To improve interface thermal conductance, graphene is chemically functionalized by groups that are compatible with the surrounding polymer.[21] To achieve the highest thermal conductivities possible, it is critically important to understand the optimal functionalization schemes. In particular, the difference in the location of functional groups (such as edge *versus* basal plane) can lead to significant differences in thermal conductivity enhancement. Recent work demonstrated that multilayer graphene is more efficient at enhancing thermal conductivity than single layer graphene.[20] For such multilayer graphene, the anisotropy in thermal conductivity can be even larger, due to weak van der Waals coupling of graphene sheets in the through-plane direction, further modifying the difference between edge and basal plane functionalization. In this work, we demonstrate that

[a] *School of Aerospace and Mechanical Engineering, University of Oklahoma, Norman, 73019, USA. E-mail: rajumenr@ou.edu*
[b] *Department of Geosciences, Stony Brook University, Stony Brook, New York 11794-2100, USA*

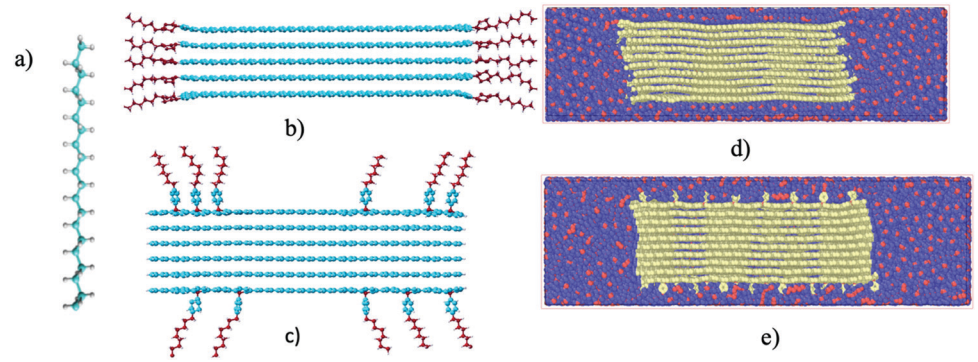

Fig. 1 (a) Polyethylene chain, (b and c) edge and basal-plane functionalized graphene nanoplatelet, and (d and e) edge and basal plane functionalized graphene nanoplate embedded in polyethylene.

functionalization on the edges can lead to significantly higher effective thermal conductivity of the polymer nanocomposite compared to functionalization on the basal plane. Detailed understanding of the effect is achieved through molecular dynamics as well as first-principles simulations based on density functional theory. The presented results unravel promising new avenues for achieving high thermal conductivity polymer–graphene nanocomposites.

The benefit of edge-bonding is found to be related to enabling all graphene sheets to be covalently bonded to surrounding polymer chains, as the edges of all sheets are exposed to the surrounding polymer (Fig. 1a). High in-plane thermal conductivity of individual sheets ($\sim$2000 W mK^{-1})[11,12] combined with their efficient coupling with the surrounding polymer through edge functionalization leads to an efficient thermal conduction pathway across the GnPs (Fig. 1b). Since all sheets are efficiently coupled with polymer through edge bonding, the entire nanoplatelet is efficient in conducting heat through edge functionalization (Fig. 1b). For basal plane bonding, however, a higher density of functional groups can be expected to attach to the basal planes of the outermost layers of the nanoplatelet (Fig. 1c). The weak van der Waals coupling of outer layers with inner layers then renders the inner layers to be less efficient in heat transfer due to the poor through-thickness thermal conductivity of graphene ($\sim$10 W mK^{-1})[19,21] (Fig. 1c). The lower heat transfer capability of inner layers for basal plane bonding can cause the overall nanoplatelet heat conduction to be lower for basal plane bonding, relative to edge bonding.

Several studies have reported enhancement of thermal conductivity through functionalization schemes. Two orders of magnitude increase in interface thermal conductance[22] and 156% enhancement[23] in thermal conductivity of the composite were achieved through grafting of polymer chains on to graphene. Theoretical studies on polymer grafted graphene showed two-fold higher interfacial thermal conductance through functional groups.[22] Similarly a pyrene-end poly(glycidyl methacrylate) functionalized graphene/epoxy composite achieved $\sim$184% enhancement in k due to noncovalent functionalization.[23] Konatham *et al.*[24] demonstrated $\sim$50% reduction in the interfacial thermal resistance between octane and functionalized graphene using a molecular dynamics (MD) simulations study. Lin *et al.*[25] explored the enhancement of out-of plane thermal conductance of graphene facilitated by the functional group of alkyl-pyrene on graphene *via* MD simulations. According to Ganguli *et al.*[26] silane-functionalized graphene improved the thermal conductivity by 50% compared to a pristine graphene composite for 8% filler content. Xiang *et al.*[27] also compared edge *versus* basal plane functionalization of graphene for energy conversion and energy storage applications. However, there is a lack of detailed understanding of the relative effectiveness of edge *versus* basal plane functionalization in enhancing the thermal conductivity of polymer–graphene nanocomposites. In particular, the role of different parameters such as nanoplatelet thickness, functional group density and functional group length in modifying the relative effectiveness of edge and basal plane functionalization is not well understood.

This study addresses the relative role of edge and basal plane functionalization in enhancing thermal conductivity through molecular dynamics simulations and first principles driven atomistic Green's function methods. Computational studies are also performed to understand the beneficial effects of edge bonding on – (a) the thermal conductivity of individual graphene sheets (using MD simulations), (b) interface thermal conductance at individual junctions between graphene and the polymer (performed using first principles driven atomistic Green's function method) and (c) damping of vibrations in the outer layers of a graphene nanoplatelet.

2. Methods

2.1 Molecular dynamics simulations

Molecular dynamics simulations were performed using the LAMMPS package.[28] Interatomic force interactions between various atomic species were modeled using the COMPASS force-field.[29] This force field has been widely used in the past to simulate polymer systems.[29] The polymer used for computational studies is polyethylene (PE) (Fig. 1a). To compare the edge and basal plane case computationally, we first functionalized the graphene nanoplatelet separately on its edges and basal plane to achieve edge (Fig. 1b) and basal plane functionalized (Fig. 1c) nanoplatelets. These functionalized nanoplatelets were then

embedded into the polyethylene matrix (using the PACKMOL package[30]) to yield edge functionalized (Fig. 1d) and basal plane functionalized (Fig. 1e) polyethylene–graphene nanocomposites. The lateral dimensions of the GnPs used for simulations were 10 nm × 10 nm while their thickness was varied from 4 to 10 layers. The polymer–graphene composite was prepared with a graphene nanoplatelet concentration of 35 wt%. The chain length of polyethylene used was 120 carbon atoms. The system was relaxed using an *NPT* ensemble (constant number of particles, pressure and temperature) to achieve an equilibrium configuration. Simulations were performed at 300 K. A temperature difference of 50 K was imposed across the composite (using Langevin thermostats[31]) and simulations were performed until a steady state was reached (typically after 5 ns). Upon reaching the steady state the resulting heat flux was computed and compared for edge and basal plane functionalization cases. To validate our models, we simulated the thermal conductivity of pure polyethylene with a density of 0.898 g cm^{-3} and obtained a value of 0.3 W mK^{-1} at 300 K which is in good agreement with simulations[9,17,32,33] and experimental results.[34,35]

2.2 Atomistic Green's function (AGF) method

To compare interface thermal conductance for a junction (between the functional group and graphene) located on edge *versus* basal plane, we used first-principles atomistic Green's function (AGF).[36,37] This method offers several unique advantages for computation of interface conductance such as allowing the use of accurate interatomic force interactions derived from density functional theory as well as the use of exact interfacial atomic arrangement. This method further enables detailed microscopic understanding of interfacial thermal transport in terms of transmission of individual phonon modes across the junction. For AGF calculations, the system is divided into left contact lead, a central interface region and right contact lead. In this work, the left lead was comprised of a polyethylene chain, the right lead was graphene nanoribbon and the central region was comprised of the junction between the polymer and graphene (Fig. 2). Phonon interface thermal conductance is computed using the Landauer formalism[38] from the estimate of phonon transmission rates. For this work, second-order interatomic force constants needed for the computation of phonon transmission were derived using the open source DFT package QUANTUM-ESPRESSO.[39] Green's functions provide a response of the system under a small perturbation and allow computation of phonon transmission across the interfacial region. Under harmonic approximation, the Green's function G—corresponding to the interfacial region—can be calculated as[40] $G_{d,d} = [\omega^2 I - H_{d,d} - \sum_R - \sum_L]$, where ω is the phonon frequency, $H_{d,d}$ represents the dynamical matrix of the interfacial region, and $\sum_L$ and $\sum_R$ are the self-energies of the left and right reservoirs which represent the effect of contact reservoirs on the interfacial region. Total phonon transmission across the interfacial region can be calculated as $\Xi(\omega) = \mathrm{Trace}[\Gamma_L G_{d,d} \Gamma_R G_{d,d}^{+}]$ where Γ_R and Γ_L describe the rate at which phonons enter and exit the right and left contact leads

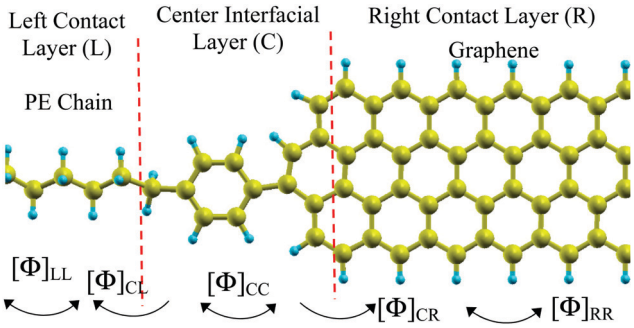

Fig. 2 Atomic configuration for atomistic Green's function calculation of interfacial thermal conductance.

respectively, $\Gamma_L = \sum_R i\left[\sum_L - \sum_L^{+}\right]$, $\Gamma_R = i\left[\sum_R - \sum_R^{+}\right]$, and '+' denotes the conjugate transpose of the matrix. The interface thermal conductance can then be calculated with the Landauer formalism using the total phonon transmission,

$$J = \int \left(\frac{\hbar\omega}{2\pi}\right) \Xi(\omega) \frac{\mathrm{d}N(\omega)}{\mathrm{d}T} \mathrm{d}\omega$$

where $N(\omega)$ and T are the Bose-Einstein population and temperature, respectively.

Harmonic interatomic force constant (IFC) matrices [ϕ] (as shown in Fig. 2) and the masses of atoms in the various layers are the only inputs needed to compute the various quantities involved in the calculation of thermal conductance. The harmonic force constant matrix $[\Phi_{ij}]_{\alpha\beta}$, between two regions α and β (α, β = L, R or C) is comprised of the interatomic force interaction Φ_{ij} between any atom i in region α and another atom j in region β. These force constants Φ_{ij} are the second derivatives of energy with respect to the displacements of atoms i and j. In this work these IFCs are derived accurately from density functional theory (DFT) using perturbation theory.[39] The use of DFT has been shown to yield very accurate IFCs in previous studies.[41] In our calculations, the right contact layer is the graphene nanoribbon and the left contact layer is a single chain of polyethylene while the center layer consists of the interfacial junction.

We first used DFT to optimize the structures of the polyethylene chain and graphene nanoribbon (ZGNR) as seen in Fig. 2. The electronic structure of PE is computed using a 10 × 1 × 1 Monkhorst-Pack *k*-grid and local density approximation is used for the exchange correlation. The width of the ZGNR is taken to be 4 zigzag chains across the nanoribbon (4-ZGNR). The edges of the ZGNR are passivated with hydrogen in this study. For computing the electronic structure of 4-ZGNR, the unit cell of ZGNR was relaxed and 30 k-points along the 1-D direction of the Brillouin zone were used for DFT calculations. Phonons of both PE and ZGNR are computed on a 12 × 1 × 1 *q*-grid, using the DFPT package; these are then used to obtain the interatomic force constants (IFCs) in real space. The IFCs derived for a single PE chain and 4-ZGNR are used for the left and right contacts, respectively. The IFCs within the interfacial region and between the interfacial region and the left and right contacts are derived by using a finite-difference approach. To compute the IFC between an

interfacial atom and any other atom in the system through this approach, the interfacial atom is displaced by a small amount. The force on the other atom resulting from this displacement is computed. The IFC is taken to be the negative of the derivative of the force on the particular atom in the system with respect to the displacement of the interfacial atom. The calculation of IFCs related to the interfacial region is discussed next. Ultrasoft pseudopotentials were used for deriving the configurations. An energy cut-off of 60 Ry was used for the wavefunctions and that of 480 Ry was used for charge density.

To understand differences in phonon transmission for the edge and basal plane cases, we used a polarization dependent AGF method. Through this approach, the contributions of individual polarizations of graphene and polyethylene to the overall transmission can be analyzed.[42] To achieve this decomposition, it should be noted that matrices Γ_L and Γ_R can be written as $\Gamma_L = \phi_{LC}A_L\phi_{CL}$ and $\Gamma_R = \phi_{RC}A_R\phi_{CR}$, where ϕ are the force interaction matrices as discussed earlier. In these expressions matrix A is proportional to phonon density of states and can be written in terms of its eigenvectors and eigenvalues as[42] $A = \sum_i \lambda_i e_i e_i^+$, where λ_i and e_i are the eigenvalues and eigenvectors of matrix A respectively.[42] The above decomposition of matrix A allows Γ_L and Γ_R to be replaced with polarization dependent phonon escape rates defined as $\gamma_L = \phi_{LC}\lambda_{L,}e_{L,}e_{L,}^+\phi_{CL}$, $\gamma_R = \phi_{RC}\lambda_{R,}e_{R,}e_{R,i}^+\phi_{CR}$. This allows phonon transmission from the left into specific phonon polarizations on the right to be written as $\xi(\omega) = \mathrm{Trace}[\Gamma_L G_{d,d}\gamma_R G_{d,d}^+]$. In this work, we take the phonon escape rates for out-of-plane and in-plane vibration modes in the right contact to be

$$\gamma_R^{\mathrm{out(in)}} = \phi_{RC}\left[\sum_{i,i\in \mathrm{out\ (in)}} \lambda_{R,i}e_{R,i}e_{R,i}^+\right]\phi_{CR}$$

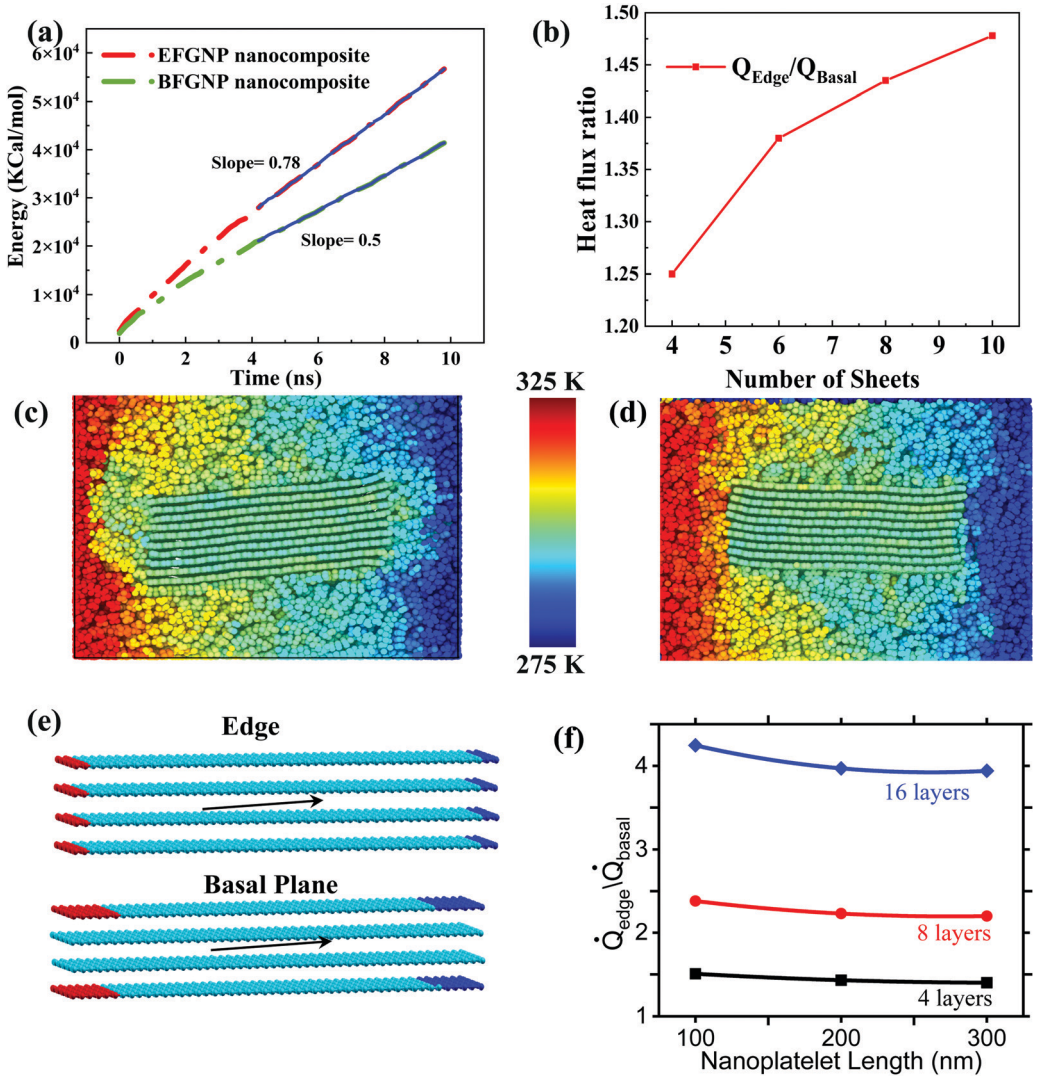

Fig. 3 (a) Energy transfer *vs.* time for edge and basal plane functionalized nanocomposites and (b) heat flux ratio for edge *vs.* basal functionalized nanocomposite as a function of nanoplatelet thickness, (c) EFGNP/PE and (d) BFGNP/PE nanocomposites. (e) Temperature boundary conditions to simulate heat flux through a single nanoplatelet for edge and basal plane functionalization (arrows show the direction of heat flow). (f) The heat flux ratio of different lengths of nanoplatelets shows higher heat flux for edge bonding.

The transmission from the polymer into the out-of-plane and in-plane vibration modes in graphene can then be computed as $\xi^{out}(\omega) = \mathrm{Trace}[\Gamma_L G_{d,d} \gamma_R \gamma_R^{out} G_{d,d}^{+}]$ and $\xi^{in}(\omega) = \mathrm{Trace}[\Gamma_L G_{d,d} \gamma_R \gamma_R^{in} G_{d,d}^{+}]$.

3. Results and discussion

3.1 Molecular dynamics simulations

The heat flux through the composite (for both edge and basal plane cases) was calculated from the slope of the "energy exchange *versus* time" graph using the equation, $J = \Delta E/(A \cdot \Delta t)$, where ΔE is the change in energy, A is the cross-sectional area and Δt is the time over which ΔE is computed. These calculations were performed using the linear portion of the graph (which corresponds to the steady state). Energy exchange (ΔE) with time is shown in Fig. 3a for the composites prepared with edge functionalized (EFGNP) and basal-plane functionalized (BFGNP) graphene nanoplatelets. The results of heat flux computation show a significant increase of nearly 48% for heat flux for the EFGNP/PE nanocomposite case over the BFGNP/PE nanocomposite case for the 10 layers thick nanoplatelet (Fig. 3b). The enhancement in heat flux is found to be thickness dependent (Fig. 3b), with thicker nanoplatelets demonstrating a larger advantage of edge relative to basal plane functionalized cases. While for 4 sheet thick nanoplatelets, the EFGNP/PE composite has 25% higher heat flux compared to the BFGNP/PE composite, increasing the sheet thickness to 10 layers, which increases the difference in heat flux to 48%. These data provide a first computational understanding of the superior effect of edge-bonding in enhancing polymer–graphene nanocomposite thermal conductivity.

This higher heat flux is mainly due to all layers of the graphene nanoplatelet being efficiently coupled to the polymer matrix leading to lower interfacial thermal resistance for the edge bonding case (Fig. 1b). For the basal plane case, however, only the outermost layers are the dominant heat conductors, as they are covalently bonded with the surrounding polymer (Fig. 1c). For this case, inner layers interact with the outer layers through weak van der Waals forces, diminishing heat transfer from the outer to inner layers, thus diminishing the contribution of inner layers to overall heat transfer for the basal plane case. This degrades the heat transfer performance for the basal plane functionalized graphene nanoplatelet. These differences in heat transfer reflect in the temperature profiles across the nanocomposite for the two cases; for the edge case, the temperature profile is significantly smoother at the interface (at the edge) between the graphene and polymer (Fig. 3c), relative to the basal plane case (Fig. 3d), where a sudden temperature jump is seen across the nanoplatelet edge. This indicates a smaller interface thermal resistance for the edge functionalization case, resulting in a higher effective thermal conductivity.

While the above simulations study the entire nanocomposite, we also performed simulations for a single nanoplatelet (Fig. 3e and f) to demonstrate the effect more clearly. Fig. 3e shows a single graphene nanoplatelet with the thermostats applied across either the edges of the entire nanoplatelet (to simulate edge bonding) or across only the outermost layers (to simulate basal plane bonding). These thermostats establish a temperature gradient of 50 K. Fig. 3f shows a comparison of the heat transfer rate between the edge and basal plane case. The edge case is seen to outperform the basal plane case as seen by the ratio ($\dot{Q}_{edge}/\dot{Q}_{basal}$) being greater than 1. It is further seen that the advantage of edge bonding (indicated by the heat transfer rate ratio) increases with increasing number of layers (n) within the nanoplatelet. While for a 4-layer thick nanoplatelet, the heat transfer rate ratio is $\sim$1.5, and this ratio increases sharply to more than 4 for a 16-layer thick nanoplatelet. The increase in difference between the edge and basal plane functionalized case with an increase in n can be understood by realizing that for the basal plane functionalized nanoplatelet, increasing the number of inner layers does not result in a significant increase in overall heat transfer rate, since the inner layers do not conduct heat efficiently due to being poorly coupled with outermost layers (which receive heat through functionalization). For the edge case, however, since all layers conduct heat efficiently, an increase in n leads to a proportional increase in overall heat transfer. This causes the ratio of heat transfer for the edge and basal plane functionalization to increase with the number of graphene sheets. This also explains the increase in heat flux ratio for edge and basal plane cases with an increase in thickness for the nanocomposite (Fig. 3b). Fig. 4 shows the effect of grafting density (0.25–1%) and number of backbone carbon atoms in the functionalized chain on thermal conductivity enhancement of the nanocomposite. It is observed that the difference in heat flux increases with an increase in both grafting density and number of carbon atoms and saturates at 1%, in good agreement with previous works.[43,44] At a higher number of backbone carbon atoms, functionalized molecules bend and fold, increasing the interface thermal resistance.[44] Hence, we observed a maximum difference in heat flux of 48% at 1% grafting density and with 12 backbone carbon atoms.

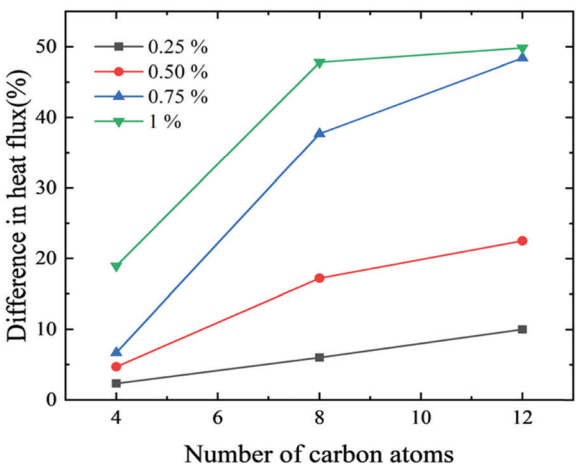

Fig. 4 Effect of grafting density and number of backbone carbon atoms in the functionalized chain, on the difference in heat flux between the edge and basal plane functionalized composites.

While the above results demonstrate the advantage of edge bonding in enhancing thermal conductivity through the coupling effect of all graphene layers to the polymer, we next present other advantages of edge bonding, namely, (a) lower damping of vibrations in graphene layers by the surrounding polymer for the edge bonding case, (b) higher thermal conductivity of individual edge-functionalized graphene sheets (studied using MD), (c) higher interface thermal conductance at an individual junction between the polymer and graphene on the edge compared to the basal plane (studied using first-principles atomistic Green's function analysis).

We first discuss the effect of edge bonding on the damping of vibrations within graphene sheets. Vibrational power density spectrum[18] is a powerful method to study damping of vibrations in graphene sheets and is computed from the discrete Fourier transform of the velocity autocorrelation function as

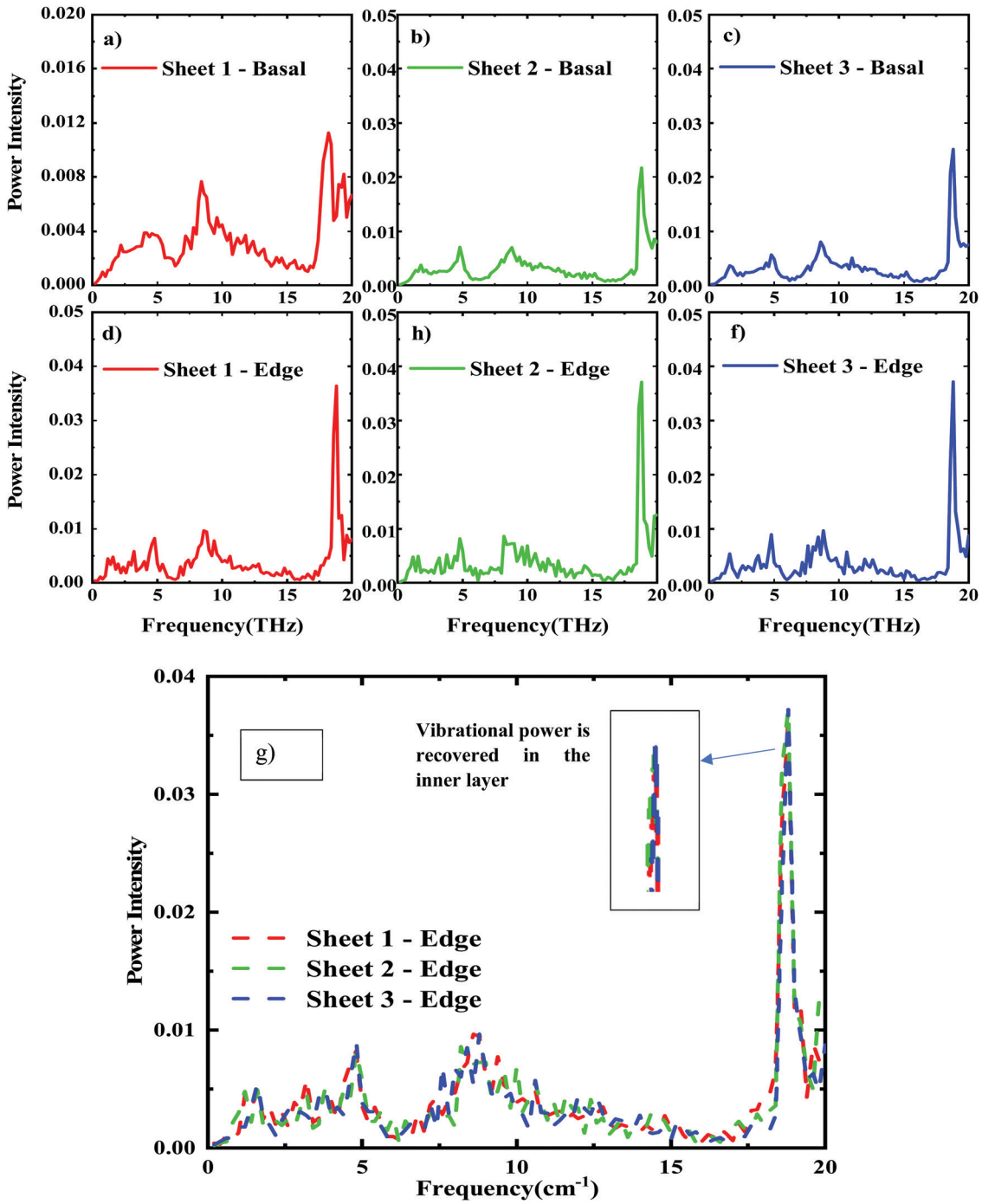

Fig. 5 (a–g) Vibrational power spectra across different layers in EFGNP and BFGNP.

shown below,

$$D(\omega) = \int_0^{\tau} \langle v(0) \cdot v(t) \rangle \exp(-i\omega t) \mathrm{d}t \quad (1)$$

where $\langle v(0) \cdot v(t) \rangle$ is the velocity autocorrelation obtained by correlating the velocity at every 2 fs time interval, τ is the total correlation time = 5 ps and $D(\omega)$ is the phonon vibrational power spectra at frequency ω.

Fig. 5a–g shows the difference in vibrational power spectra for edge and basal plane functionalization cases for a 6 sheet nanoplatelet (embedded in the polymer matrix). The power spectra are presented for individual sheets within the nanoplatelet. Sheet 1 denotes the outermost layer from the bottom. We have shown the vibrational power spectra of sheets 1–3. We focus on vibrational power density at a frequency of around 18 THz.[45] Comparing Fig. 5a and d, it is seen that the vibrational power in Sheet 1 (outermost sheet) is lower in BFGNP than EFGNP by almost a factor of 3.5. This stronger damping of vibrations in the outermost sheet for the BFGNP case is caused by a strong covalent-bond mediated interaction between the outer sheet and polymer for the BFGNP case, in contrast to the case of edge bonding where the interactions are much weaker caused by van der Waals forces.

The vibrational power for the inner sheets is also higher for the edge case compared to basal plane functionalization. The inner layers for the edge case do not have a large contact area with the surrounding polymers (only interact through edges) and therefore are less damped compared to the outer sheet, causing a small increase in their power density (see the inset in Fig. 5g) relative to outer sheet. The inner sheets for the edge case at the same time receive heat from edges through strong covalent bonds. For the basal plane case, however, vibrational power for the inner sheets stays lower relative to the edge case. This is simply due to the weak van der Waals interaction of the inner layer with the outer layer for the basal plane case which causes poor heat transfer to the inner layers for the basal plane case. The above comparison of the vibrational power density spectrum highlights the significant advantages of edge bonding for heat conduction.

We next compare the effect of edge and basal plane bonding on the thermal conductivity of individual graphene sheets. Edge-bonding is found to enable remarkably superior thermal

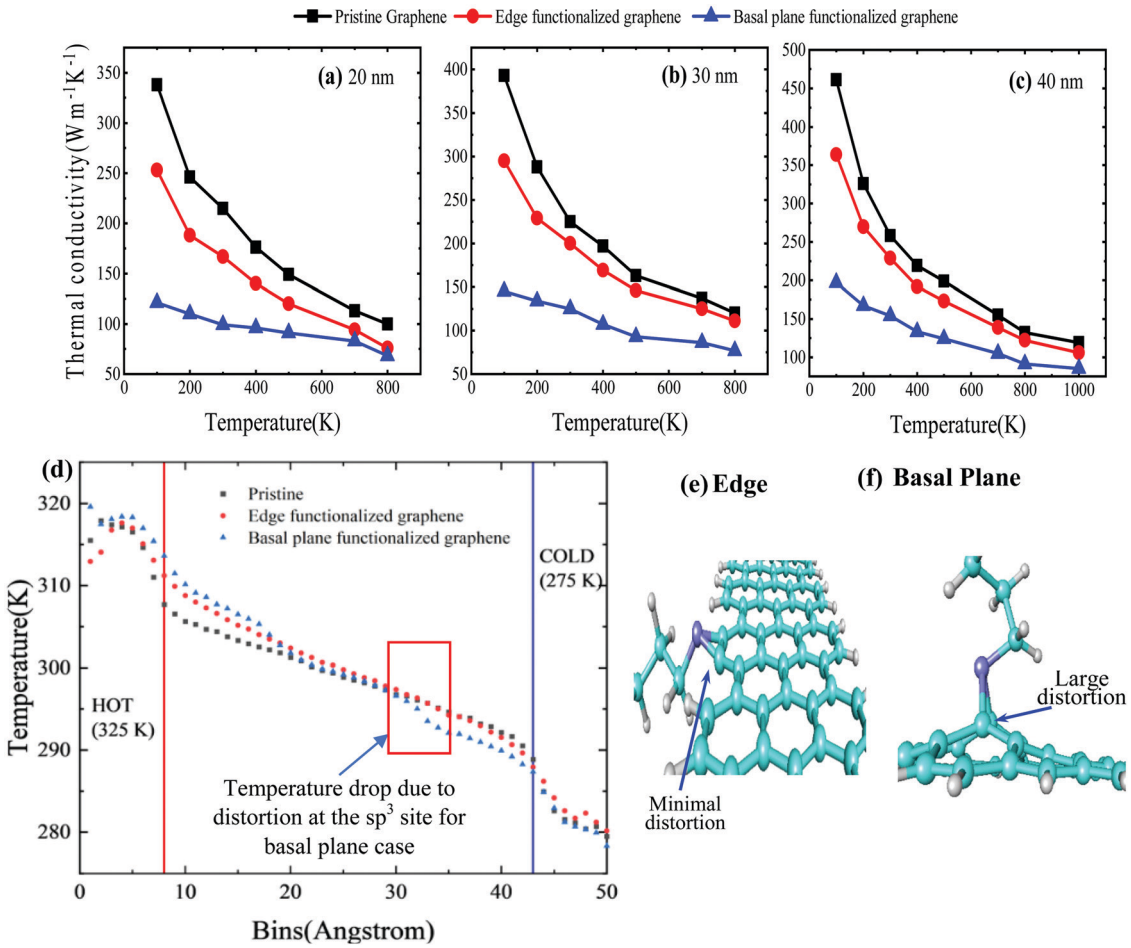

Fig. 6 Temperature dependence of thermal conductivity for pristine, edge functionalized and basal plane functionalized graphene with lateral dimensions of (a) 20 nm, (b) 30 nm, and (c) 40 nm. (d) Temperature distribution along the simulation box in pristine, edge, and basal plane functionalized graphene. The relaxed atomic configurations for (e) edge and (f) basal plane functionalization demonstrate larger distortion of graphene for basal plane functionalization.

conductivity of individual graphene sheets relative to basal plane functionalization (Fig. 6). For the pristine graphene case, k at nanometer length scales is found to be in good agreement with previous works.[46] At a length scale of 20 nm and at room temperature (300 K), the thermal conductivity (k) of pristine, edge functionalized, and basal plane functionalized graphene are computed to be 215 W mK^{-1}, 167 W mK^{-1}, and 99 W mK^{-1}, respectively. The thermal conductivity predicted for the edge-functionalized case is 68.7% higher than the basal plane case and 28.7% lower than pristine graphene. This reduction in thermal conductivity upon functionalization (relative to pristine graphene) is due to the distortion of the graphene structure. The large reduction in thermal conductivity in basal plane functionalization is attributed to much larger distortion of graphene in its basal plane as shown in Fig. 6f. Edge bonding distorts graphene to a much smaller degree compared to the basal plane case, as seen in the relaxed DFT (density-functional theory) structures in Fig. 6e and f. Carbon atoms on the basal plane of graphene are sp^2 hybridized; in forming an extra bond to functionalize, they transform to the sp^3 state, protruding outwards and distorting graphene in the process. Unlike inner carbon atoms, edge atoms can adopt tetrahedral geometries

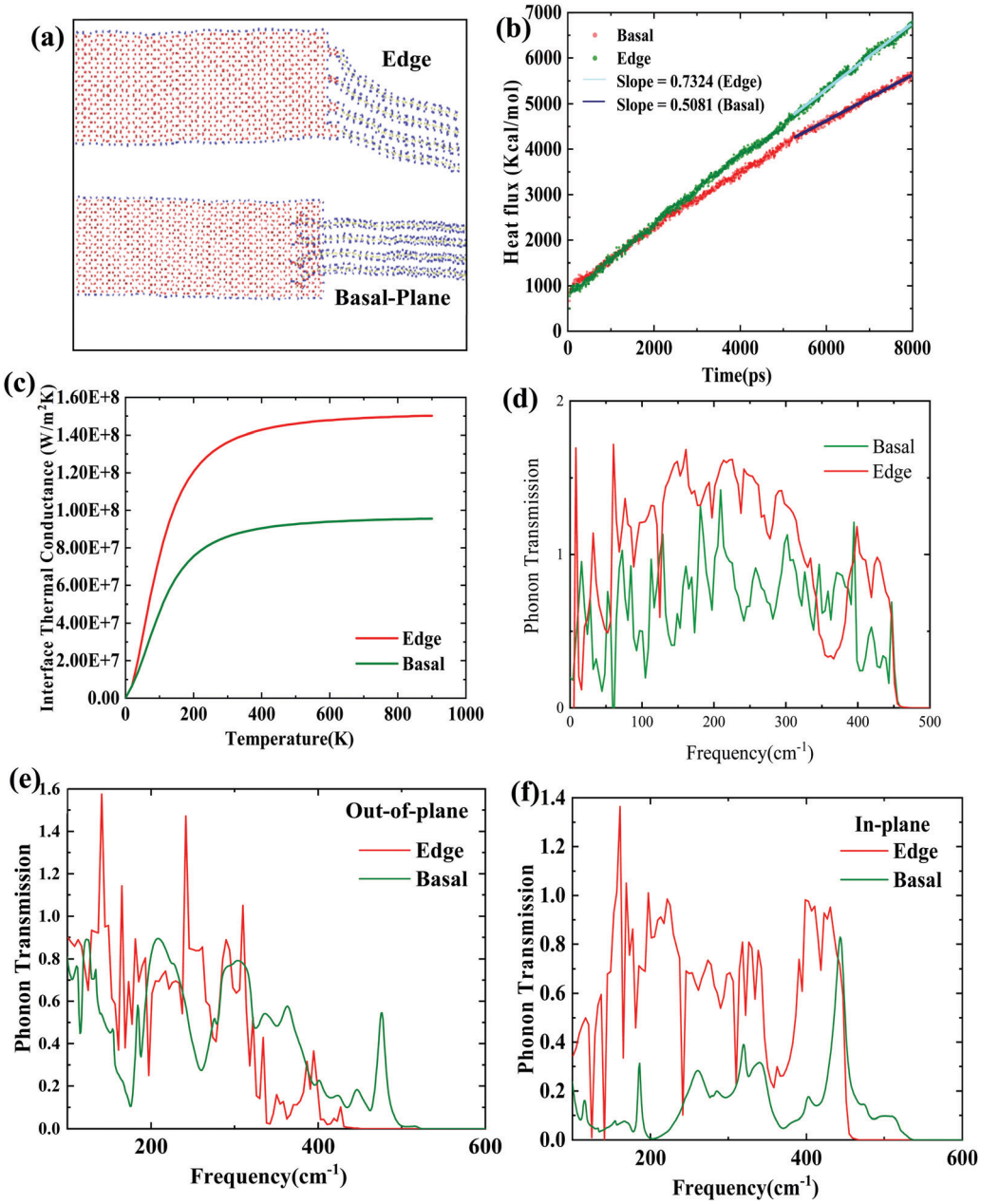

Fig. 7 (a) Junction involving a polymer chain bonded on the edge and basal plane of graphene. Comparison between the edge and basal plane functionalization in terms of (b) heat flux across a junction, (c) interface thermal conductance and (d) overall phonon transmission. Comparison between the edge and basal plane in terms of transmission to (e) in-plane phonons and (f) out of-plane phonons of graphene.

more freely without causing extra strain. Lower distortion through edge bonding results in significantly higher $k_{graphene}$ relative to the basal plane case. To demonstrate this effect clearly, we present the temperature along the length of the graphene sheet for pristine, edge functionalized and basal plane functionalized graphene. We have divided the graphene (100 Å long) into 50 bins. For the basal plane case, a sudden temperature drop at the functionalized sites is observed, indicating a reduction in thermal conductivity due to phonon scattering at functionalization sites. However, temperature distribution within the edge functionalized graphene remains linear due to the minimal distortion and shows no such sudden temperature drop. These results clearly demonstrate that edge functionalized graphene has a superior heat conduction ability compared to basal plane functionalized graphene.

While the above results demonstrate advantage of edge bonding in heat conduction in individual graphene sheets, we next demonstrate that interface thermal conductance is also higher at an individual junction (between polymer chain and graphene) located on the edge of graphene as opposed to on the basal plane. This implies that heat conducts into graphene more efficiently through a junction located on the edge compared to the basal plane. Molecular dynamics simulations were used to compare interface thermal conductance for the junction at an edge relative to on the basal plane. Atomic structures for the two cases are shown in Fig. 7a which shows polymer chains bonded on the edge as well as on the basal plane of graphene. A temperature difference of 20 K was applied across the location of bonding (junction) and the resulting heat flux was computed. MD computations reveal almost 40% higher heat flux for the edge case relative to the basal plane case (Fig. 7b). Understanding of this higher interface thermal conductance is achieved using first-principles Green's function calculations, described next.

3.2 Atomistic Green's function computations

Fig. 7c shows that the AGF method also predicts almost 60% higher interface thermal conductance for the edge case relative to basal plane bonding at 300 K. This agrees qualitatively with MD simulation results.

Fig. 7d shows that this higher thermal conductance is due to the higher phonon transmission for a junction on the edge of graphene relative to the basal plane. To understand this higher phonon transmission for the edge case, we split the total phonon transmission from the polymer chain into the in-plane and out-of-plane vibration modes of graphene using the polarization dependent atomistic Green's function method (details provided in the Methods section). The results show that transmission from polymer to in-plane vibration modes of graphene is much larger for the edge case relative to basal plane bonding. The contribution of out-of-plane vibration modes to total transmission is found to be comparable for edge and basal plane bonding cases. This higher transmission to in-plane phonons of graphene for the edge case leads to the higher overall phonon transmission for the edge relative to basal plane cases, resulting in higher interfacial thermal conductance for the edge case. The above computations provide a comprehensive understanding of the higher polymer–graphene nanocomposite thermal conductivity through edge relative to basal plane functionalization.

4. Conclusion

In summary, this work provides a detailed comparison of edge and basal plane functionalization of graphene nanoplatelets in enhancing the thermal conductivity of the polymer–graphene nanocomposite, through both molecular dynamics study and Green's function calculations. Edge bonding is shown to lead to superior enhancement in the thermal conductivity of the composite relative to basal plane bonding. Molecular dynamics simulations reveal this advantage of edge bonding to be due to all sheets of graphene nanoplatelets interacting efficiently with the surrounding polymer through edge bonding. Coupling of the high in-plane thermal conductivity of graphene ($\sim$2000 W mK^{-1}) with the surrounding polymer through edge bonding leads to an efficient thermal conduction pathway through the composite. For basal plane bonding, only the outermost layers (surface layers) of the nanoplatelet have significant thermal interaction with the polymer. Poor out-of-plane thermal conductivity of graphene ($\sim$10 W mK^{-1}) causes inefficient heat conduction from the outer to inner layers, resulting in the overall nanoplatelet being less effective in heat conduction for basal plane bonding compared to edge bonding. Overall, simulations predict 48% higher k through the edge relative to basal plane bonding, at 35 wt% composition and for 10 layer thick nanoplatelets. Simulations further reveal other advantages of edge bonding, such as lower damping of vibrations in all layers of the nanoplatelet through edge bonding, high thermal conductivity of individual graphene layers through minimal distortion of the graphene structure induced by edge functionalization, and higher thermal conductance of the individual junction at the edge relative to the basal plane, mediated by higher phonon transmission to in-plane phonons of graphene. This work opens up new avenues to achieve higher thermal conductivity of polymer–graphene nanocomposites, with important applications in a wide range of thermal management technologies.

Conflicts of interest

There are no conflicts of interest to declare.

Acknowledgements

R. M., F. T., S. D. and J. G. acknowledge support from the National Science Foundation CAREER award under Award No. #1847129. We also acknowledge the University of Oklahoma Supercomputing Center for Education and Research (OSCER) for providing computing resources for this work.

References

1 S. Mallik, N. Ekere, C. Best and R. Bhatti, Investigation of thermal management materials for automotive electronic control units, *Appl. Therm. Eng.*, 2011, **31**, 355–362.

2 J.-K. Lee, Y.-J. Lee, W.-S. Chae and Y.-M. Sung, Enhanced ionic conductivity in PEO-LiClO 4 hybrid electrolytes by structural modification, *J. Electroceram.*, 2006, **17**, 941–944.

3 Z. Shang, H. Qi, X. Liu, C. Ouyang and Y. Wang, Structural optimization of lithium-ion battery for improving thermal performance based on a liquid cooling system, *Int. J. Heat Mass Transfer*, 2019, **130**, 33–41, DOI: **10.1016/j.ijheatmasstransfer.2018.10.074**.

4 B. Ravdel, *et al.*, Thermal stability of lithium-ion battery electrolytes, *J. Power Sources*, 2003, **119–121**, 805–810, DOI: **10.1016/S0378-7753(03)00257-X**.

5 W. U. Huynh, J. J. Dittmer and A. P. Alivisatos, Hybrid nanorod-polymer solar cells, *Science*, 2002, **295**, 2425–2427.

6 X. Lu and G. Xu, Thermally conductive polymer composites for electronic packaging, *J. Appl. Polym. Sci.*, 1997, **65**, 2733–2738.

7 P. Procter and J. Solc, Improved thermal conductivity in microelectronic encapsulants, *IEEE Trans. Compon., Hybrids, Manuf. Technol.*, 1991, **14**, 708–713.

8 V. Singh, *et al.*, High thermal conductivity of chain-oriented amorphous polythiophene, *Nat. Nanotechnol.*, 2014, **9**, 384–390, DOI: **10.1038/nnano.2014.44**.

9 R. Muthaiah and J. Garg, Temperature effects in the thermal conductivity of aligned amorphous polyethylene—A molecular dynamics study, *J. Appl. Phys.*, 2018, **124**, 105102, DOI: **10.1063/1.5041000**.

10 M. Saeidijavash, *et al.*, High thermal conductivity through simultaneously aligned polyethylene lamellae and graphene nanoplatelets, *Nanoscale*, 2017, **9**, 12867–12873, DOI: **10.1039/C7NR04686C**.

11 A. A. Balandin, *et al.*, Superior thermal conductivity of single-layer graphene, *Nano Lett.*, 2008, **8**, 902–907.

12 S. Ghosh, *et al.*, Dimensional crossover of thermal transport in few-layer graphene, *Nat. Mater.*, 2010, **9**, 555–558.

13 F. Tarannum, R. Muthaiah, R. S. Annam, T. Gu and J. Garg, Effect of Alignment on Enhancement of Thermal Conductivity of Polyethylene–Graphene Nanocomposites and Comparison with Effective Medium Theory, *Nanomaterials*, 2020, **10**, 1291.

14 R. Muthaiah, F. Tarannum, N. Yedukondalu and J. Garg First principles investigation of high thermal conductivity in hexagonal boron phosphide. *arXiv preprint*, 2022, arXiv:2201.09430.

15 R. Muthaiah and J. Garg, First principles investigation of high thermal conductivity in hexagonal germanium carbide(2H-GeC), *Carbon Trends*, 2021, **5**, 100113, DOI: **10.1016/j.cartre.2021.100113**.

16 R. Muthaiah and J. Garg, Ultrahigh thermal conductivity in hexagonal BC6N- An efficient material for nanoscale thermal management- A first principles study, *Comput. Mater. Sci.*, 2021, **200**, 110773, DOI: **10.1016/j.commatsci.2021.110773**.

17 R. Muthaiah, *Thermal transport in polymers, polymer nanocomposites and semiconductors using molecular dynamics simulation and first principles study*, 2021.

18 K. M. Shahil and A. A. Balandin, Graphene–multilayer graphene nanocomposites as highly efficient thermal interface materials, *Nano Lett.*, 2012, **12**, 861–867.

19 M. Saeidijavash, *et al.*, High thermal conductivity through simultaneously aligned polyethylene lamellae and graphene nanoplatelets, *Nanoscale*, 2017, **9**, 12867–12873.

20 X. Shen, *et al.*, Multilayer graphene enables higher efficiency in improving thermal conductivities of graphene/epoxy composites, *Nano Lett.*, 2016, **16**, 3585–3593.

21 A. A. Balandin, Thermal properties of graphene and nanostructured carbon materials, *Nat. Mater.*, 2011, **10**, 569–581.

22 M. Wang, D. Galpaya, Z. B. Lai, Y. Xu and C. Yan, Surface functionalization on the thermal conductivity of graphene–polymer nanocomposites, *Int. J. Smart Nano Mater.*, 2014, **5**, 123–132.

23 C.-C. Teng, C.-C. M. Ma, K.-C. Chiou and T.-M. Lee in 2010 5th International Microsystems Packaging Assembly and Circuits Technology Conference. 1–4 (IEEE).

24 D. Konatham and A. Striolo, Thermal boundary resistance at the graphene-oil interface, *Appl. Phys. Lett.*, 2009, **95**, 163105.

25 S. Lin and M. J. Buehler, The effect of non-covalent functionalization on the thermal conductance of graphene/organic interfaces, *Nanotechnology*, 2013, **24**, 165702.

26 S. Ganguli, A. K. Roy and D. P. Anderson, Improved thermal conductivity for chemically functionalized exfoliated graphite/epoxy composites, *Carbon*, 2008, **46**, 806–817.

27 Z. Xiang, Q. Dai, J. F. Chen and L. Dai, Edge functionalization of graphene and two-dimensional covalent organic polymers for energy conversion and storage, *Adv. Mater.*, 2016, **28**, 6253–6261.

28 S. Plimpton, Fast Parallel Algorithms for Short-Range Molecular Dynamics, *J. Comput. Phys.*, 1995, **117**, 1–19, DOI: **10.1006/jcph.1995.1039**.

29 H. Sun, COMPASS: An ab Initio Force-Field Optimized for Condensed-Phase ApplicationsOverview with Details on Alkane and Benzene Compounds, *J. Phys. Chem. B*, 1998, **102**, 7338–7364, DOI: **10.1021/jp980939v**.

30 L. Martínez, R. Andrade, E. G. Birgin and J. M. Martínez, PACKMOL: a package for building initial configurations for molecular dynamics simulations, *J. Comput. Chem.*, 2009, **30**, 2157–2164.

31 J. Liu, D. Li and X. Liu, A simple and accurate algorithm for path integral molecular dynamics with the Langevin thermostat, *J. Chem. Phys.*, 2016, **145**, 024103.

32 T. Evgin, *et al.*, Size effects of graphene nanoplatelets on the properties of high-density polyethylene nanocomposites: morphological, thermal, electrical, and mechanical characterization, *Beilstein J. Nanotechnol.*, 2020, **11**, 167–179.

33 R. Muthaiah and J. Garg, in APS March Meeting Abstracts. F49. **013**.

34 S. Zhang, *et al.*, The effects of particle size and content on the thermal conductivity and mechanical properties of Al_2O_3/high density polyethylene (HDPE) composites, *Express Polymer Lett.*, 2011, **5**, 581–590.

35 T. A. Osswald, E. Baur, S. Brinkmann, K. Oberbach and E. Schmachtenberg, *International plastics handbook*, Hanser, Munich, 2006, vol. 758, p. 67.

36 C. Caroli, R. Combescot, P. Nozieres and D. Saint-James, Direct calculation of the tunneling current, *J. Phys. C-Solid State Phys.*, 1971, **4**, 916.
37 Y. Meir and N. S. Wingreen, Landauer formula for the current through an interacting electron region, *Phys. Rev. Lett.*, 1992, **68**, 2512.
38 R. Landauer, Electrical resistance of disordered one-dimensional lattices, *Philos. Mag.*, 1970, **21**, 863–867.
39 P. Giannozzi, *et al.*, QUANTUM ESPRESSO: a modular and open-source software project for quantum simulations of materials, *J. Phys.: Condens. Matter*, 2009, **21**, 395502.
40 W. Zhang, T. Fisher and N. Mingo, The atomistic Green's function method: an efficient simulation approach for nanoscale phonon transport, *Numer. Heat Transfer, Part B*, 2007, **51**, 333–349.
41 S. Baroni, S. De Gironcoli, A. Dal Corso and P. Giannozzi, Phonons and related crystal properties from density-functional perturbation theory, *Rev. Mod. Phys.*, 2001, **73**, 515.
42 Z. Huang, J. Y. Murthy and T. S. Fisher, Modeling of Polarization-Specific Phonon Transmission through Interfaces, *J. Heat Transfer*, 2011, **133**, 114502.
43 Y. Gao and F. Müller-Plathe, Increasing the Thermal Conductivity of Graphene-Polyamide-6,6 Nanocomposites by Surface-Grafted Polymer Chains: Calculation with Molecular Dynamics and Effective-Medium Approximation, *J. Phys. Chem. B*, 2016, **120**, 1336–1346, DOI: **10.1021/acs.jpcb.5b08398**.
44 P. Ding, *et al.*, Influence on thermal conductivity of polyamide-6 covalently-grafted graphene nanocomposites: varied grafting-structures by controllable macromolecular length, *RSC Adv.*, 2014, **4**, 18782–18791, DOI: **10.1039/C4RA00500G**.
45 P. Yuan, P. Zhang, T. Liang, S. Zhai and D. Yang, Effects of functionalization on energy storage properties and thermal conductivity of graphene/n-octadecane composite phase change materials, *J. Mater. Sci.*, 2019, **54**, 1488–1501.
46 M. S. Islam, I. Mia, S. Ahammed, C. Stampfl and J. Park, Exceptional in-plane and interfacial thermal transport in graphene/2D-SiC van der Waals heterostructures, *Sci. Rep.*, 2020, **10**, 1–16.

